

Analytical theory of grating couplers for waveguide sensing: a perturbational approach and its limitations

R. Horvath*, L. C. Wilcox[§], H. C. Pedersen*, N. Skivesen*,
J. S. Hesthaven[§], and P. M. Johansen*

**Optics and Plasma Research Department, Risø National Laboratory,
DK-4000 Roskilde, Denmark*

*§Division of Applied Mathematics, Brown University,
Providence, RI 02912, USA*

ABSTRACT

The in-coupling process for grating-coupled planar optical waveguide sensors is investigated in the case of TE waves. A simple analytical model based on the Rayleigh-Fourier method is applied together with a perturbational technique to calculate analytical expressions for the guided wave amplitudes. In addition, analytical expressions are derived for the position correction and width of the in-coupling resonant peaks. Numerical computations verify the model for shallow gratings both in terms of peak shape and position and provide the limitations for the analytical formulas.

1. Introduction

The application of grating couplers in planar optical waveguides was introduced by Lukosz and Tiefenthaler¹ in 1983 as transducer elements for biological and chemical sensing. Since the introduction of this concept a vast amount of scientific effort has been invested into the experimental and theoretical characterization of the grating coupler in terms of optimizing its sensitivity²⁻⁸.

In most cases, the grating coupler consists of a sinusoidal or square-wave-formed surface corrugation embedded in the waveguiding film, implying that the actual thickness of the film varies periodically in the grating region. This thickness modification alters the mode properties of the waveguide as compared to those of a non-corrugated waveguide. In the literature, this influence is often neglected, as the grating amplitude is considered small in comparison with the film thickness.⁹⁻¹⁴ However, Kunz *et al.*¹⁵ exposed the importance of finite grating depths for high sensitivity grating-coupled waveguide sensors by using a rigorous numerical analysis. The aim of the present paper is to analyze the influence of the grating depth analytically by using a perturbational approach based on the pioneering work of Kiselev¹⁶ in 1975. Finally, we investigate the regions of validity of the analytical model by comparing it with numerical results obtained using a boundary variation method.¹⁷⁻¹⁹

2. Wave propagation in a corrugated waveguide: homogeneous problem

In most grating-coupled waveguide sensors a coupling-grating imprinted into the waveguiding film is illuminated by an external light source while the amount of light coupled into the waveguide is being detected. However, as we shall see, most of the characteristic sensor properties are given solely by the waveguide geometry irrespective of the manner in which it is being illuminated. In this section we therefore start by solving Maxwell's equations for a waveguide,

which is left isolated without being illuminated from the outside. This is referred to as the homogeneous problem.

A. Basic assumptions

The system considered is shown in Fig. 1. Here a waveguiding film with thickness d_F and refractive index n_F is embedded between a semi-infinite substrate with refractive index n_S and a semi-infinite cover medium with refractive index n_C . The film-cover interface is corrugated with a sinusoidal grating profile h of the form

$$h(x) = \sigma \sin(Kx), \quad K = 2\pi/\Lambda, \quad (1)$$

where σ is the grating amplitude, K is the grating wave number, and Λ is the period of the grating.

In the case where no light is incident upon the waveguide, there will only be downwards propagating waves in the substrate, i.e. waves with negative z components of the wave vector, and only upwards propagating waves in the cover. In the film, however, both up- and downwards propagating waves are present due to reflections at the interfaces.

We assume that in each medium one dominating zeroth-order wave with an x component of the wave vector k_x is present. Apart from that, diffracted waves are present due to diffraction off the grating. However, the surface corrugation amplitude σ is taken to be small (smallness to be quantified later) so that only the $\pm 1^{\text{st}}$ diffraction orders in each medium are taken into account. This assumption is well known from the Rayleigh-Fourier analysis of optical diffraction in

gratings, which is valid when the grating depth is much smaller than the light wavelength. As a result, a total of twelve waves are included in our analysis, as illustrated in Fig. 2.

Like in the conventional three-layer waveguide analysis without surface corrugation,²⁰ we wish to end up with a mode equation that dictates which values of k_x (i.e. which modes) are allowed in the waveguide. It should be emphasized here that a mode in our case consists of a set of twelve waves rather than the traditional four waves considered for non-corrugated waveguides.

We restrict the analysis to cover only TE polarized waves, which is sufficient to illustrate the main features of the corrugated waveguide.

B. Solution ansatz

Since all three media are considered homogeneous, isotropic, and non-magnetic, we know that Maxwell's equations have simple plane-wave solutions. Hence, for the TE polarized electric fields we may use the following scalar solution ansatz for the fields in the substrate, film, and cover

$E_{S,F,C}$:

$$\begin{aligned}
 E_S &= \sum_{l=-1}^1 b_l^- \exp[i(k_x + lK)x - ik_{z,l}^S z], \\
 E_F &= \sum_{l=-1}^1 \{a_l^+ \exp[i(k_x + lK)x + ik_{z,l}^F z] + a_l^- \exp[i(k_x + lK)x - ik_{z,l}^F z]\}, \\
 E_C &= \sum_{l=-1}^1 b_l^+ \exp[i(k_x + lK)x + ik_{z,l}^C z].
 \end{aligned} \tag{2}$$

The temporal frequency term $\exp(-i\omega t)$ has been omitted for simplicity, and l is a summation index that runs through the diffraction-order numbers $-1, 0,$ and 1 . b_l^- are the amplitudes of the

three diffraction orders in the substrate, where the superscript "-" refers to downwards propagating waves, a_l^+ and a_l^- are the corresponding amplitudes of the up- and downwards propagating waves in the film, and b_l^+ are the upwards propagating wave amplitudes in the cover. As mentioned, k_x denotes the x component of the zeroth-order wave vectors, which is identical in all three media, and $k_{z,l}^j$ ($j = S, F, C$) represent the z components of the individual wave vectors defined by

$$k_{z,l}^j = \sqrt{k_0^2 n_j^2 - (k_x + lK)^2} . \quad (3)$$

Here we have the vacuum wavenumber $k_0 = 2\pi/\lambda_0$, λ_0 is the vacuum wavelength, and n_j are the refractive indices of substrate, film, and cover, respectively.

C. Boundary conditions

To work out which values of k_x are allowed in the waveguide we need to apply the well-known boundary conditions stating that the tangential components of the electric and magnetic fields are continuous across the substrate-film and film-cover boundaries.

(i) Continuity of tangential electric field at substrate-film boundary

By matching the expressions of E_S and E_F from Eqs. (2) at the boundary $z = -d_F$ we obtain the following three relations:

$$b_l^- \exp(ik_{z,l}^S d_F) = a_l^+ \exp(-ik_{z,l}^F d_F) + a_l^- \exp(ik_{z,l}^F d_F), \quad (4)$$

where $l = -1, 0, 1$. As is seen here, the initial equation $E_S(z = -d_F) = E_F(z = -d_F)$ is split up into three equations in Eq. (4), which is a result of the orthogonality of the spatial harmonics $\exp[i(k_x + lK)x]$. Therefore, the coefficients of each space-harmonic can be collected and set to zero separately resulting in three equations relating the nine amplitudes b_l^- , a_l^+ , and a_l^- ($l = -1, 0, 1$).

(ii) *Continuity of tangential magnetic field at substrate-film boundary*

From the assumption that the electric field \vec{E} is TE polarized, i.e. $\vec{E} = \hat{y}E$, and that the media involved are homogeneous, isotropic, and non-magnetic it follows from Maxwell's equations that the magnetic field \vec{H} is proportional to $\hat{x}\partial_z E - \hat{z}\partial_x E$, where \hat{x}, \hat{z} are unit vectors along the x and z directions and $\partial_{x,z}$ are derivatives with respect to x and z , respectively. The tangential part of \vec{H} is then found simply by scalar multiplying with the tangential surface vector $\vec{t} = \hat{x} + \hat{z}\partial_x h$ (see Fig. 1) resulting in

$$H_{\text{Tangential}} \propto \partial_z E - \partial_x E \partial_x h, \quad (5)$$

where h represents the surface topography defined in Eq. (1).

At the substrate-film boundary $\partial_x h$ is obviously zero, which leaves us with a simple matching between $\partial_z E_S|_{z=-d_F}$ and $\partial_z E_F|_{z=-d_F}$ leading to

$$k_{z,l}^S b_l^- \exp(ik_{z,l}^S d_F) = -k_{z,l}^F a_l^+ \exp(-ik_{z,l}^F d_F) + k_{z,l}^F a_l^- \exp(ik_{z,l}^F d_F), \quad (6)$$

where again $l = -1, 0, 1$ and the coefficients of the spatial harmonics $\exp[i(k_x + lK)x]$ have been collected and set to zero. Like in Eqs. (4), Eqs. (6) comprise three equations relating the nine amplitudes b_l^- , a_l^+ , and a_l^- ($l = -1, 0, 1$).

(iii) *Continuity of tangential electric field at film-cover boundary*

By matching E_F and E_C from Eqs. (2), now at the boundary $z = \sigma \sin(Kx)$, we obtain:

$$\begin{aligned} \sum_{l=-1}^1 \left(\{a_l^+ \exp[ik_{z,l}^F \sigma \sin(Kx)] + a_l^- \exp[-ik_{z,l}^F \sigma \sin(Kx)]\} \exp[i(k_x + lK)x] \right) = \\ \sum_{l=-1}^1 \{b_l^+ \exp[ik_{z,l}^C \sigma \sin(Kx)] \exp[i(k_x + lK)x]\}. \end{aligned} \quad (7)$$

If we assume that the grating is shallow, i.e. $\sigma \ll 1/k_{z,l}^j$, we may use the relation $\exp[ik_{z,l}^j \sigma \sin(Kx)] \approx 1 + ik_{z,l}^j \sigma \sin(Kx)$ and obtain

$$\begin{aligned} \sum_{l=-1}^1 \left(a_l^+ \left\{ 1 + \frac{k_{z,l}^F \sigma}{2} [\exp(iKx) - \exp(-iKx)] \right\} \exp(ilKx) + \right. \\ \left. a_l^- \left\{ 1 - \frac{k_{z,l}^F \sigma}{2} [\exp(iKx) - \exp(-iKx)] \right\} \exp(ilKx) \right) = \\ \sum_{l=-1}^1 \left(b_l^+ \left\{ 1 + \frac{k_{z,l}^C \sigma}{2} [\exp(iKx) - \exp(-iKx)] \right\} \exp(ilKx) \right), \end{aligned} \quad (8)$$

in which the common factor $\exp(ik_x x)$ has been omitted. After expanding the sum in Eq. (8), constant terms (i.e. terms that do not depend on x) as well as terms proportional to $\exp(-iKx)$ and $\exp(iKx)$ are collected and set to zero. This results in three equations relating the nine amplitudes

a_l^+ , a_l^- , and b_l^+ ($l = -1,0,1$). Terms of higher order being proportional to $\exp(-2iKx)$ and $\exp(2iKx)$ are omitted, as they relate to diffraction orders that are neglected.

(iv) *Continuity of tangential magnetic field at film-cover boundary*

By using relation (5) to match $H_{Tangential}$ at the film-cover boundary we obtain

$$\begin{aligned}
& \sum_{l=-1}^1 k_{z,l}^F a_l^+ \left\{ 1 + \frac{k_{z,l}^F \sigma}{2} [\exp(iKx) - \exp(-iKx)] \right\} \exp(ilKx) - \\
& \sum_{l=-1}^1 k_{z,l}^F a_l^- \left\{ 1 - \frac{k_{z,l}^F \sigma}{2} [\exp(iKx) - \exp(-iKx)] \right\} \exp(ilKx) - \\
& \frac{K\sigma}{2} \sum_{l=-1}^1 (k_x + lK) (a_l^+ + a_l^-) [\exp(iKx) + \exp(-iKx)] \exp(ilKx) = \\
& \sum_{l=-1}^1 k_{z,l}^C b_l^+ \left\{ 1 + \frac{k_{z,l}^C \sigma}{2} [\exp(iKx) - \exp(-iKx)] \right\} \exp(ilKx) - \\
& \frac{K\sigma}{2} \sum_{l=-1}^1 (k_x + lK) b_l^+ [\exp(iKx) + \exp(-iKx)] \exp(ilKx) ,
\end{aligned} \tag{9}$$

where again the common factor $\exp(ik_x x)$ has been omitted and terms proportional to σ^2 have been neglected.

Like in Eq. (8) constant terms as well as terms proportional to $\exp(-iKx)$ and $\exp(iKx)$ are collected and set to zero resulting in yet another three equations relating a_l^+ , a_l^- , and b_l^+ ($l = -1,0,1$).

D. Deriving the mode equation

As mentioned above, each of the four boundary conditions generates three equations which add up to twelve equations relating the twelve field amplitudes a_l^+ , a_l^- , b_l^+ , and b_l^- ($l = -1, 0, 1$). However, by combining Eqs. (4) and (6) it is possible to isolate the amplitudes of the downwards propagating waves in the form:

$$a_l^- = \beta_l a_l^+, \quad b_l^- = \gamma_l a_l^+,$$

$$\beta_l = \frac{k_{z,l}^F + k_{z,l}^S}{k_{z,l}^F - k_{z,l}^S} \exp(-2ik_{z,l}^F d_F), \quad \gamma_l = 2 \frac{k_{z,l}^F}{k_{z,l}^F - k_{z,l}^S} \exp[-i(k_{z,l}^F + k_{z,l}^S) d_F]. \quad (10)$$

Using these expressions in Eqs. (8) and (9) the number of equations can be reduced to six with the six unknowns a_l^+ , b_l^+ ($l = -1, 0, 1$). After some algebraic manipulation of this system of equations we arrive at the following matrix equation

$$\mathbf{A} \vec{e} = \vec{0}, \quad (11)$$

where $\vec{e} = \{a_0^+, a_1^+, a_{-1}^+, b_0^+, b_1^+, b_{-1}^+\}$ and the elements of \mathbf{A} are given by

$$\begin{aligned}
A_{11} &= 1 + \beta_0, \quad A_{12} = -\frac{\sigma}{2} k_{z,1}^F (1 - \beta_1), \quad A_{13} = \frac{\sigma}{2} k_{z,-1}^F (1 - \beta_{-1}), \quad A_{14} = -1, \\
A_{15} &= \frac{\sigma}{2} k_{z,1}^C, \quad A_{16} = -\frac{\sigma}{2} k_{z,-1}^C, \quad A_{21} = \frac{\sigma}{2} k_{z,0}^F (1 - \beta_0), \quad A_{22} = 1 + \beta, \\
A_{23} &= 0, \quad A_{24} = -\frac{\sigma}{2} k_{z,0}^C, \quad A_{25} = -1, \quad A_{26} = 0, \\
A_{31} &= -\frac{\sigma}{2} k_{z,0}^F (1 - \beta_0), \quad A_{32} = 0, \quad A_{33} = 1 + \beta_{-1}, \quad A_{34} = \frac{\sigma}{2} k_{z,0}^C, \\
A_{35} &= 0, \quad A_{36} = -1, \quad A_{41} = k_{z,0}^F (1 - \beta_0), \\
A_{42} &= -\frac{\sigma}{2} \left[(k_{z,1}^F)^2 + (k_x + K)K \right] (1 + \beta_1), \\
A_{43} &= \frac{\sigma}{2} \left[(k_{z,-1}^F)^2 - (k_x - K)K \right] (1 + \beta_{-1}), \quad A_{44} = -k_{z,0}^C, \\
A_{45} &= \frac{\sigma}{2} \left[(k_{z,1}^C)^2 + (k_x + K)K \right], \quad A_{46} = -\frac{\sigma}{2} \left[(k_{z,-1}^C)^2 - (k_x - K)K \right], \\
A_{51} &= \frac{\sigma}{2} \left[(k_{z,0}^F)^2 - k_x K \right] (1 + \beta_0), \quad A_{52} = k_{z,1}^F (1 - \beta_1), \\
A_{53} &= 0, \quad A_{54} = -\frac{\sigma}{2} \left[(k_{z,0}^C)^2 - k_x K \right], \quad A_{55} = -k_{z,1}^C, \quad A_{56} = 0, \\
A_{61} &= -\frac{\sigma}{2} \left[(k_{z,0}^F)^2 + k_x K \right] (1 + \beta_0), \quad A_{62} = 0, \\
A_{63} &= k_{z,-1}^F (1 - \beta_{-1}), \quad A_{64} = \frac{\sigma}{2} \left[(k_{z,0}^C)^2 + k_x K \right], \quad A_{65} = 0, \quad A_{66} = -k_{z,-1}^C.
\end{aligned} \tag{12}$$

To obtain nontrivial solutions to Eq. (11) the determinant of \mathbf{A} must equal zero. This results in a mode equation that can be written in the following form by keeping only terms up to σ^2 :

$$\begin{aligned}
D_0 D_1 D_{-1} &= \\
&+ \frac{\sigma^2}{2} k_{z,0}^F (k_{z,0}^F - k_{z,0}^C) \left[\sum_{l=\pm 1} \frac{(k_{z,l}^F)^2 - (k_{z,l}^C)^2}{(1 - \beta_l) k_{z,l}^F - (1 + \beta_l) k_{z,l}^C} (1 + \beta_l) - 2k_{z,0}^C \right] D_1 D_{-1} \\
&+ \frac{\sigma^2}{2} \left[\left(\frac{T}{2} - K^2 \right) D_1 D_{-1} + \sum_{l=\pm 1} M_l (1 + \beta_l) D_{-l} \right] D_0,
\end{aligned} \tag{13}$$

$$D_l = k_{z,l}^C (1 + \beta_l) - k_{z,l}^F (1 - \beta_l),$$

$$M_l = \frac{1}{2} \left[(k_{z,l}^F)^2 (k_{z,0}^C - k_{z,0}^F - k_{z,l}^C) + (k_{z,l}^C)^2 (k_{z,0}^F - k_{z,0}^C) + (k_{z,l}^C)^3 \right],$$

$$T = -(k_{z,1}^C)^2 - 2k_{z,0}^F k_{z,0}^C - (k_{z,-1}^C)^2.$$

Here D_l ($l = -1, 0, 1$) are the individual determinants of the three groups of diffraction orders for the non-corrugated waveguide ($\sigma = 0$). For example, D_0 represents the determinant of the 4×4 matrix that would have resulted if only the zeroth order waves a_0^+ , a_0^- , b_0^+ , and b_0^- had been present in a non-corrugated waveguide. Hence, the equation $D_0 = 0$ is equivalent to the conventional 3-layer mode equation for a planar waveguide without grating.^{16,20} The terms proportional to σ^2 on the right hand side of Eq. (13) are small correction terms representing the influence of the grating on the modes.

E. Solving the mode equation: perturbational approach

The mode equation (13) describes those values of k_x (corresponding to propagation angles in the waveguide) that make the original solution ansatz, Eq. (2), with twelve waves a solution to Maxwell's equations.

Usually, the solutions to the mode equation are expressed in terms of normalized k_x values called the effective refractive index $N = k_x/k_0$. In general, a number of distinct solutions N_m exist for each waveguide geometry, with m being the mode number. In the following we shall analyze the impact of the surface corrugation on the solutions to the mode equation. Because σ is considered small, we write N_m as a sum of the non-corrugated solution $N_m(\sigma = 0) = N_m^{nc}$ and a perturbation term δN_m :

$$N_m = N_m^{nc} + \delta N_m. \quad (14)$$

By using $N_m = N_m^{nc}$ on the right hand side of Eq. (13) it is possible to recover a simplified mode equation:

$$D_0 = \frac{\sigma^2}{2} k_{z,0}^F (k_{z,0}^F - k_{z,0}^C) \left[\sum_{l=\pm 1} \frac{(k_{z,l}^F)^2 - (k_{z,l}^C)^2}{(1-r_l)k_{z,l}^F - (1+r_l)k_{z,l}^C} (1+\beta_l) - 2k_{z,0}^C \right]_{N=N_m^{nc}}. \quad (15)$$

To derive an analytical expression for δN_m we expand Eq. (15) to first order in δN_m to recover

$$\delta N_m = \delta N_m' + i\delta N_m'' = \frac{i}{k_0^2 d_{eff} N} \left(\frac{k_{z,0}^F \sigma}{2} \right)^2 \left[2k_{z,0}^C + \sum_{l=\pm 1} (k_{z,l}^F + k_{z,l}^C) \frac{\nu_l^S \exp(-2ik_{z,l}^F d_F) + 1}{\nu_l^S \nu_l^C \exp(-2ik_{z,l}^F d_F) - 1} \right]_{N=N_m^{nc}}, \quad (16)$$

$$\nu_l^j = (k_{z,l}^F + k_{z,l}^j) / (k_{z,l}^F - k_{z,l}^j), \quad j = S, C,$$

where $\delta N_m'$ and $\delta N_m''$ denote the real and imaginary parts of δN_m and d_{eff} is the effective thickness of the non-corrugated waveguide defined by²¹

$$d_{eff} = d_F + i \left(\frac{1}{k_{z,0}^C} + \frac{1}{k_{z,0}^S} \right). \quad (17)$$

In most practical sensor applications light is coupled in from air. In such cases and when $\text{Max}\{n_S, n_C\} > (n_F + 1)/2$, which is also mostly fulfilled, $\delta N_m'$ and $\delta N_m''$ can be written in the following analytical form:

$$\delta N_m' \cong \left(\frac{k_0 \sigma}{2} \right)^2 \frac{n_F^2 - N_m^2}{k_0 N_m d_{eff}} \left[-2\sqrt{N_m^2 - n_C^2} + (k_0) \frac{n_F^2 - n_C^2}{|k_{z,1}^F| + |k_{z,1}^C|} \right]_{N=N_m^{nc}}, \quad (18)$$

$$\delta N_m'' = \left(\frac{\sigma}{2} \right)^2 \frac{n_F^2 - N_m^2}{N_m d_{eff}} \frac{(n_F^2 - n_C^2) \left\{ k_{z,-1}^S (k_{z,-1}^F)^2 + k_{z,-1}^C \left[(k_0) (k_{z,-1}^S)^2 + (k_0)^3 (n_F^2 - n_S^2) \cos^2(k_{z,-1}^F d_F) \right] \right\}}{\left[(k_{z,-1}^F)^2 + k_{z,-1}^S k_{z,-1}^C \right]^2 - (k_0)^4 (n_F^2 - n_S^2) (n_F^2 - n_C^2) \cos^2(k_{z,-1}^F d_F)} \Bigg|_{N=N_m^{nc}} \quad (19)$$

In Fig. 3 $\delta N_0'$ and $\delta N_0''$ are plotted versus the corrugation depth σ for the nanoporous waveguide.^{22,23} It is seen that $\delta N_0'$ is negative implying that the mode propagation angle in the film θ , defined by $\sin(\theta) = N_0/n_F$, is decreased as a result of the surface corrugation. As expected, $\delta N_0''$ is seen to be positive. The physical consequence of this is that each of the twelve waves in the solution ansatz (2) decay with the damping factor $\exp(-k_0 \delta N_0'' x)$. This damping is due to the diffractive out-coupling of the main wave into the substrate and cover media through the $l = -1$ diffraction orders. Therefore, the radiation loss coefficient of the system is given by $\alpha_{RAD} = k_0 \delta N_m''$.

In Fig. 4, $\delta N_0'$ and $\delta N_0''$ are plotted versus film thickness d_F for a surface corrugation of $\sigma = 10$ nm. Here, it is seen that for large film thickness and a film thickness close to the cutoff, $\delta N_0'$ and $\delta N_0''$ vanish. This is due to the fact that for a large film thickness, the surface corrugation has a decreasing influence on the effective thickness, whereas for a film thickness close to cutoff, the field penetration depth into the cover medium goes to infinity, so that eventually most of the mode power propagates outside the film and therefore does not experience the surface corrugation. Mathematically both effects are described by the $1/d_{eff}$ term.

3. Coupling into the waveguide: non-homogeneous problem

In this section we assume that a monochromatic plane wave is incident on the waveguide through the substrate, see Fig. 5. In order to couple into the mode, we need to launch the wave along the -1^{st} diffraction order, i.e. with an angle of incidence θ_s given by $n_s \sin(\theta_s) = N - K/k_0$, so that after transmission through the substrate-film interface, the incident wave gets diffracted off the grating into the direction of the a_0 wave components. The resulting solution ansatz to be inserted in Maxwell's equations is therefore:

$$\begin{aligned}
E_S &= c_{-1}^+ \exp[i(k_x - K)x + ik_{z,-1}^S z] + \sum_{l=-1}^1 b_l^- \exp[i(k_x + lK)x - ik_{z,l}^S z], \\
E_F &= \sum_{l=-1}^1 \{a_l^+ \exp[i(k_x + lK)x + ik_{z,l}^F z] + a_l^- \exp[i(k_x + lK)x - ik_{z,l}^F z]\}, \\
E_C &= \sum_{l=-1}^1 b_l^+ \exp[i(k_x + lK)x + ik_{z,l}^C z],
\end{aligned} \tag{20}$$

where c_{-1}^+ is the amplitude of the incident field.

By following exactly the same procedures as in Secs. 2C and 2D, it is straightforward to obtain the following non-homogeneous matrix equation:

$$\mathbf{A}\vec{e} = \vec{c}, \tag{21}$$

where \mathbf{A} and \vec{e} are given in Sec. 2D and the driving vector \vec{c} is given by

$$\vec{c} = \begin{pmatrix} \frac{\sigma}{2} k_{z,-1}^F \\ 0 \\ -1 \\ -\frac{\sigma}{2} \left[(k_{z,-1}^F)^2 - (k_x - K) K \right] \\ 0 \\ k_{z,-1}^F \end{pmatrix} \kappa_{-1} c_{-1}^+, \quad (22)$$

with

$$\kappa_l = -\frac{k_{z,l}^S}{k_{z,l}^F} \gamma_l. \quad (23)$$

Eq. (23) is readily solved by multiplying both sides with \mathbf{A}^{-1} :

$$\vec{e} = \mathbf{A}^{-1} \vec{c}. \quad (24)$$

By keeping only the lowest order terms in σ , analytical expressions for the elements of \vec{e} can be found. For example, the amplitude a_0^+ assumes the form

$$a_0^+ = \frac{\sigma k_{z,-1}^F k_0^2 (n_F^2 - n_C^2) D_1 \kappa_{-1} c_{-1}^+}{\det(\mathbf{A})}. \quad (25)$$

The total internal reflection of the a_0^+ and a_0^- waves in the film implies that $|a_0^+| = |a_0^-|$. Thus, the in-coupled mode power is proportional to $|a_0^+|^2$. In Fig. 6 this in-coupled mode power for the nanoporous waveguide versus N is plotted for three different values of surface corrugation depth σ . First of all, it is seen that for small surface corrugations a clear resonance close to the non-

corrugated effective mode refractive index, N_0^{nc} , appears. However, the position of the resonance peak shifts downwards with increasing σ , the peak height decreases with increasing σ , and the half-width increases with σ .

These peak shape characteristics are largely described by the $1/\det(\mathbf{A})$ factor in Eq. (25). This is easily seen by Taylor expanding $\det(\mathbf{A})$ around $N = N_m$.^{24,25}

$$\det(\mathbf{A}) = C_1(N - N_m) + C_2(N - N_m)^2 + \dots, \quad (26)$$

where $C_{1,2,\dots}$ are constants. Close to resonance, i.e. $N \rightarrow N_m$, we may keep only the first order term, after which we get

$$\det(\mathbf{A}) \cong C_1 \left[N - (N_m^{nc} + \delta N_m') - i\delta N_m'' \right]. \quad (27)$$

Thus, because the square modulus of a_0^+ is proportional to $|\det(\mathbf{A})|^{-2}$, the in-coupled mode power assumes a Lorentzian shape around resonance:

$$|a_0^+|^2 \propto \frac{1}{\left[N - (N_m^{nc} + \delta N_m') \right]^2 + (\delta N_m'')^2}, \quad (28)$$

where $\delta N_m'$ represents the shift in resonance and $\delta N_m''$ determines the peak height and the half-width ($= 2\delta N_m''$) achieved due to the surface corrugation, just as we observed in Fig. 6.

4. Numerical verification

In order to verify the validity of our analytical approach above, we have analyzed the in-coupling problem numerically. The numerical routine used is the so-called multiple interface boundary variation method.¹⁷⁻¹⁹ This approach enables modeling of periodic transmission consisting of an arbitrary number of materials and interfaces of general shape subject to plane wave illumination. A convolution of the exact waveguide solution with a multi-layered boundary variation solution yields the coupling coefficient for light coupled into the sensor.

In Figs. 7a-c the results of the numerical solutions are shown as dotted data points. As can be seen, there is good correlation between the numerical data and the analytical curves for σ up to ~ 80 nm.

Regarding the peak shapes, these are further analyzed in Fig. 8 where $\delta N_0'$ (resonance position) and $\delta N_0''$ (resonance height and width) have been compared with the analytically obtained values. It is seen that the analytical model starts breaking down at $\sigma \approx 80$ nm corresponding to about 1/2 of the film thickness.

The $\delta N_0'$ and $\delta N_0''$ values may easily be converted into corresponding propagation angle values $\delta\theta_j$ ($j = S, F, C$) in the three media by using that

$$\begin{aligned}\delta\theta_j' &= \delta N_0' / n_j, \\ \delta\theta_j'' &= 2\delta N_0'' / n_j.\end{aligned}\tag{29}$$

Here $\delta\theta_j'$ and $\delta\theta_j''$ represent the shift in coupling angle and peak half-width, respectively. Thus, for $\sigma = 80$ nm, corresponding to half the film thickness, the peak shifts and peak half-widths (measured in the substrate) are 0.28 deg and 0.22 deg, respectively. Using the grating equation one can easily calculate the in-coupling angle, measured in air, which is the usual experimentally measured waveguide sensor parameter. For $\sigma = 10$ nm, a typical grating depth, the peak shift is 5.8×10^{-3} deg, which is approximately two orders of magnitude higher than the resolution usually obtained in optical waveguide lightmode spectroscopy.^{9,26}

5. Discussion

Based on the well-known Rayleigh-Fourier analysis we have analyzed the influence of finite grating depths on the TE mode properties in grating-coupled optical planar waveguide sensors. By using a perturbational approach, expressions for the in-coupling peak shift and peak width have been derived. The analytical results obtained for a specific waveguide geometry were compared with rigorous numerical calculations. It was found that for grating amplitudes up to approximately half the waveguide film thickness, the analytical model provides satisfactory results.

In the analyzed example, it was shown that a typical grating amplitude of 10 nm causes a shift on the order of 10^{-3} deg which is two orders of magnitude larger than a typical resolution for a waveguide sensor device. Hence, the finite grating depth influence is significant when performing absolute refractive index measurements or when performing absolute thickness detections of small add layers, such as proteins, lipid bilayers and inorganic film depositions.

The presented model can be extended to cover TM mode propagation too and, moreover, we believe that the method may be used for finite grating lengths also.

Acknowledgements

This work was supported by the Danish Technical Research Council, grants #26-01-0211 and #26-03-0272.

The work of Wilcox was partially supported by a National Science Foundation (NSF) sponsored Vertical Integration of Research and Education in the Mathematical Sciences program at Brown University and partially supported by the Army Research Office under contract DAAD19-01-1-0631.

The work of Hesthaven was partially supported by the Army Research Office under contract DAAD19-01-1-0631, by NSF through an NSF Career Award, and by the Alfred P. Sloan Foundation through a Sloan Research Fellowship.

References

1. W. Lukosz and K. Tiefenthaler, "Integrated optical switches and gas sensors" *Optics Letters* **10**, 137-139 (1984).
2. K. Tiefenthaler and W. Lukosz, "Sensitivity of grating couplers as integrated-optical chemical sensors" *J. Opt. Soc. Am. B* **6**, 209 (1989).
3. W. Lukosz, "Principles and sensitivities of integrated optical and surface plasmon sensors for direct affinity sensing and immunosensing", *Biosensors and Bioelectronics* **6**, 215-225 (1991).
4. W. Lukosz, "Integrated optical chemical and direct biochemical sensors," *Sens. Actuators* **29**, 37 – 50 (1995).

5. K. Tiefenthaler and W. Lukosz, "Grating couplers as integrated optical humidity and gas sensors," *Thin Solid Films*, **126**, 205 – 211 (1985).
6. K. Tiefenthaler, "Integrated optical couplers as chemical waveguide sensors", *Advances in Biosensors* **2**, 261-289 (1992).
7. O. Parriaux and P. Sixt, "Sensitivity optimization of a grating coupled evanescent wave immunosensor" sensors and Actuators B **29**, 289-292 (1995).
8. R. Horváth, L.R. Lindvold and N.B. Larsen, "Reverse symmetry waveguides. Theory and fabrication" *Applied Physics B* **74**, 383 (2002).
9. J. Voros, J. J. Ramsden, G. Csucs, I. Szendro, S. M. de Paul, M. Textor, and N. D. Spencer, "Optical grating coupler biosensors," *Biomaterials*, **23**, 3699 – 3710 (2002).
10. J. J. Ramsden, "Review of new experimental techniques for investigating random sequential adsorption" *J.Stat.Phys.* **73**, 853-877 (1993).
11. J. J. Ramsden, "Partial molar volume of solutes in bilayer lipid membranes" *J.Phys.Chem.* **97**, 4479-4483 (1993).
12. J. J. Ramsden, S.-Y. Li, J. E. Prenosil, E. Heinzle, "Kinetics of adhesion and spreading of animal-cells" *Biotechnology and Bioengineering* **43**, 939-945 (1994).
13. R. Horvath, J. Voros, R. Graf, G. Fricsovszky, M. Textor, LR Lindvold, ND Spencer and E. Papp, "Effect of patterns and inhomogeneities on the surface of waveguides used for optical waveguide lightmode spectroscopy applications", *Applied Physics B* **72**, 441-447 (2001).
14. R. Horvath, G. Fricsovszky, E. Papp, "Application of the optical waveguide lightmode spectroscopy to monitor lipid bilayer phase transition" *Biosensors and Bioelectronics* **18**, 415-428 (2003).
15. RE Kunz, J. Dubendorfer and RH Morf, "Finite grating depth effects for integrated optical sensors with high sensitivity" *Biosensors and Bioelectronics* **11**, 653-667 (1996).

16. VA Kiselev "Diffraction coupling of radiation into a thin-film waveguide" Sov. J. Quant. Electron., **4**, 872-875 (1975).
17. O. P. Bruno, and F. Reitich, "Numerical solution of diffraction problems: a method of variation of boundaries," J. Opt. Soc. Am. A **10**, 1168 – 1175 (1993).
18. O. P. Bruno, and F. Reitich, "Numerical solution of diffraction problems: a method of variation of boundaries. II. Finitely conducting gratings, Pade approximants, and singularities," J. Opt. Soc. Am. A **10**, 2307 – 2316 (1993).
19. L. C. Wilcox, P. G. Dinesen, and J. S. Hesthaven, "Fast and accurate boundary variation method for multi-layered diffraction optics," J. Opt. Soc. Am. A, to appear (2004).
20. P. K. Tien, "Integrated optics and new wave phenomena in optical waveguides" Rev. Modern Phys. **49**, 361 (1977).
21. H. Kogelnik and H. P. Weber, "Rays, stored energy, and power flow in dielectric waveguides," J. Opt. Soc. Am. **64**, 174 – 185 (1974).
22. R. Horvath, H.C. Pedersen, and N.B. Larsen, "Demonstration of reverse symmetry waveguide sensing in aqueous solutions" Appl. Phys. Lett. **81**, 2166-2168 (2002).
23. R. Horvath, H. C. Pedersen, N. Skivesen, D. Selmeczi, and N. B. Larsen, "Optical waveguide sensor for on-line monitoring of bacteria," Opt. Lett. **28**, 1233 - 1235 (2003).
24. A. K. Ghatak, K. Thyagarajan, and M. R. Shenoy, "Numerical analysis of planar optical waveguides using matrix approach" IEEE J. Lightwave Technol. **LT-5**, 660 (1987).
25. M. R. Ramadas, E. Garmire, A. K. Ghatak, K. Thyagarajan, and M. R. Shenoy, "Analysis of absorbing and leaky planar waveguides: a novel method," Opt. Lett. **14**, 376 – 378 (1989).

Figure Captions

Fig. 1. Schematic illustration of the waveguide structure considered. $n_{s,F,C}$ are the refractive indices of the substrate, film and cover media, respectively, σ is the grating amplitude, \vec{t} is a tangential vector at the film-cover interface, Λ is the grating period, and d_F is the film thickness.

Fig. 2. Diffraction orders included in the homogeneous analysis.

Fig. 3. Real and imaginary parts of the correction term δN_0 plotted against surface corrugation depth σ for a nanoporous waveguide.^{22,23} The parameters used are $n_S = 1.22$, $n_F = 1.57$, $n_C = 1.33$, $\lambda_0 = 632.8$ nm, $\Lambda = 480$ nm, and $d_F = 160$ nm.

Fig. 4. Real and imaginary parts of the correction term δN_0 plotted against film thickness d_F for a nanoporous waveguide.^{22,23} The parameters used are: $n_S = 1.22$, $n_F = 1.57$, $n_C = 1.33$, $\lambda_0 = 632.8$ nm, $\Lambda = 480$ nm, and $\sigma = 10$ nm.

Fig. 5. Wave vector scheme for the non-homogeneous case, in which an external wave with amplitude c_{-1}^+ is incident on the waveguiding film through the substrate.

Fig. 6. In-coupled mode power versus effective refractive index N for the nanoporous waveguide (data given in Fig. 3 and 4).

Fig. 7. In-coupled mode intensity versus effective refractive index N for the nanoporous waveguide (data given in Figs. 3 and 4). Line: analytical, points: numerical.

Fig. 8. $\delta N'$ and $\delta N''$ versus grating amplitude obtained analytically and numerically.

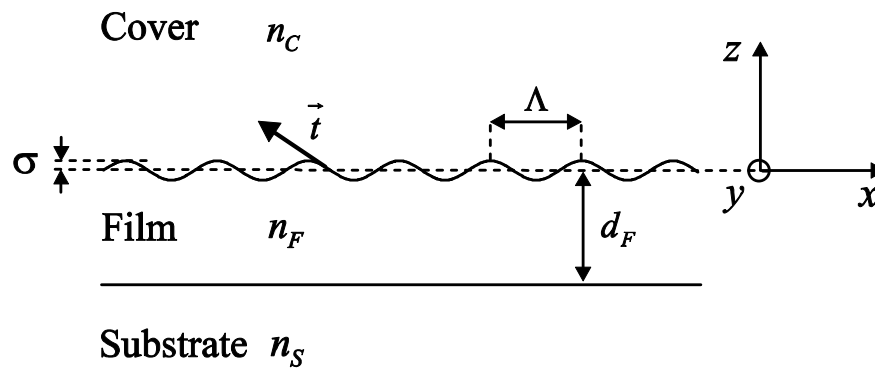


Fig. 1, Horvath et al, JOSA B

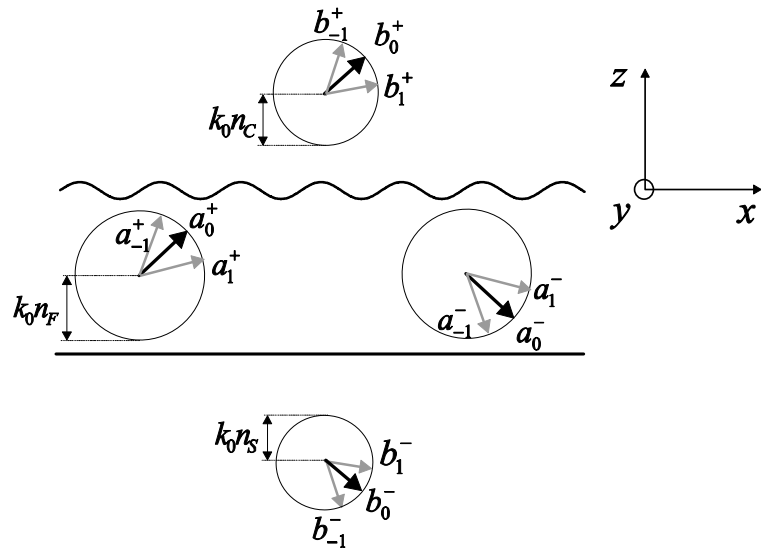


Fig. 2. Horvath et al., JOSA B

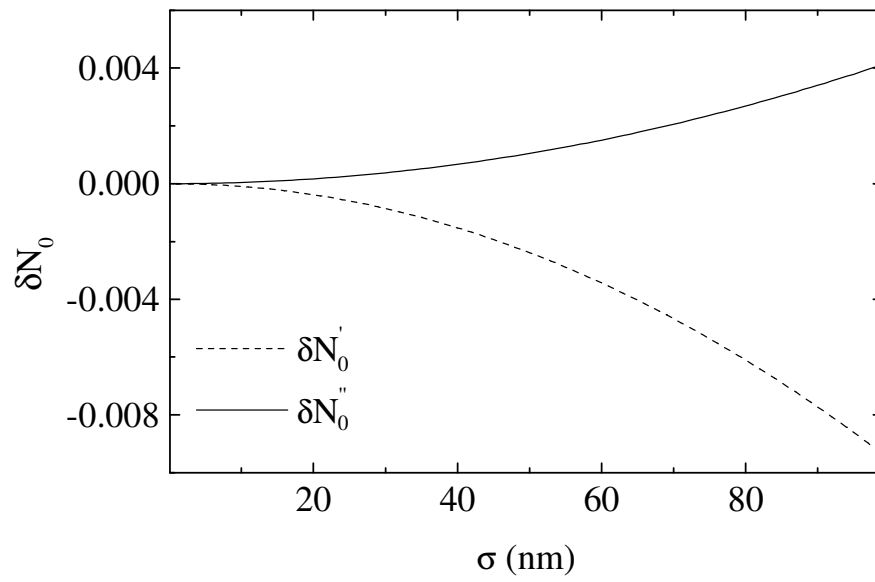


Fig. 3. Horvath et al., JOSA B

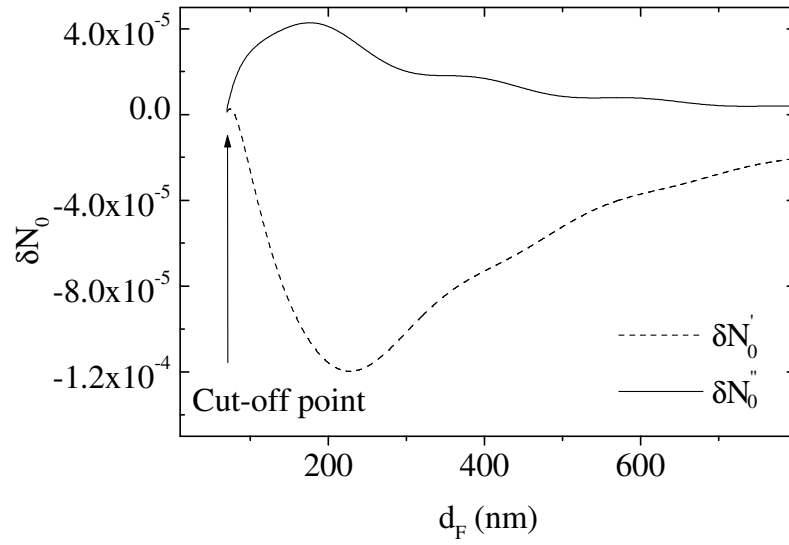


Fig. 4. Horvath et al., JOSA B

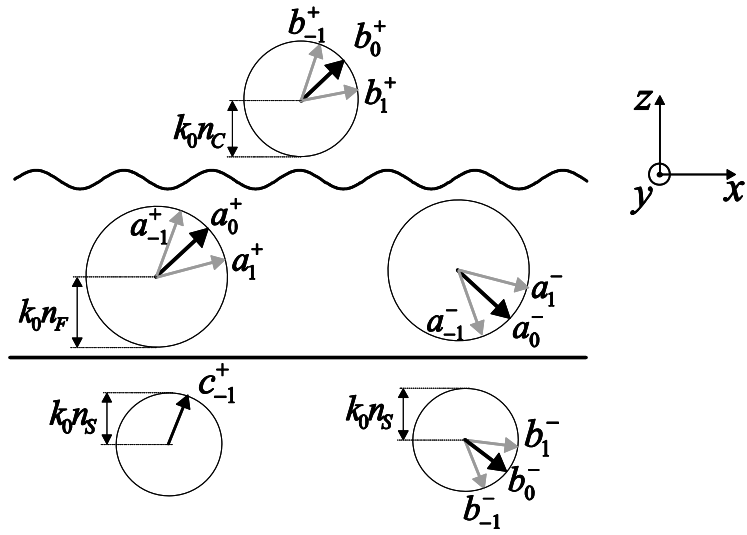


Fig. 5. Horvath et al., JOSA B

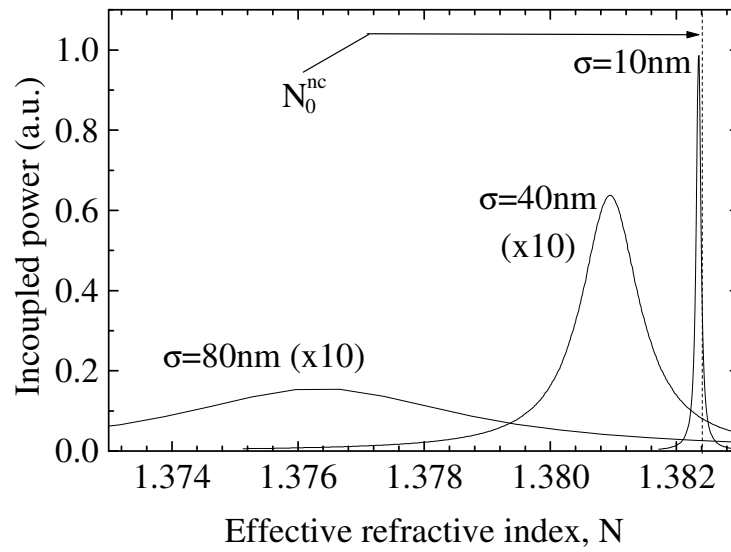
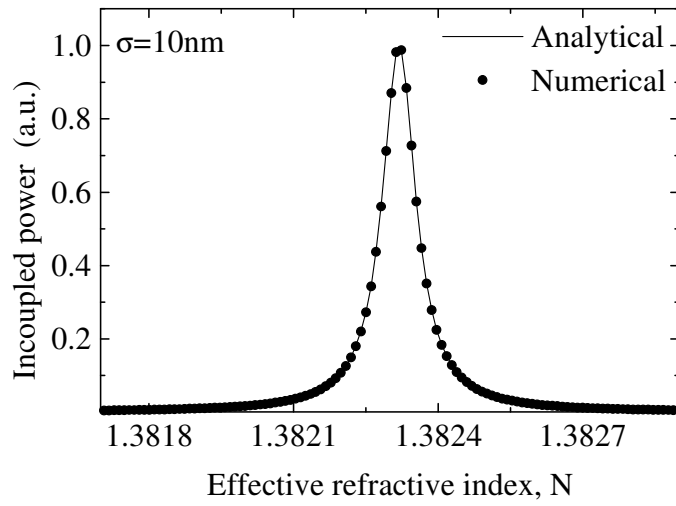
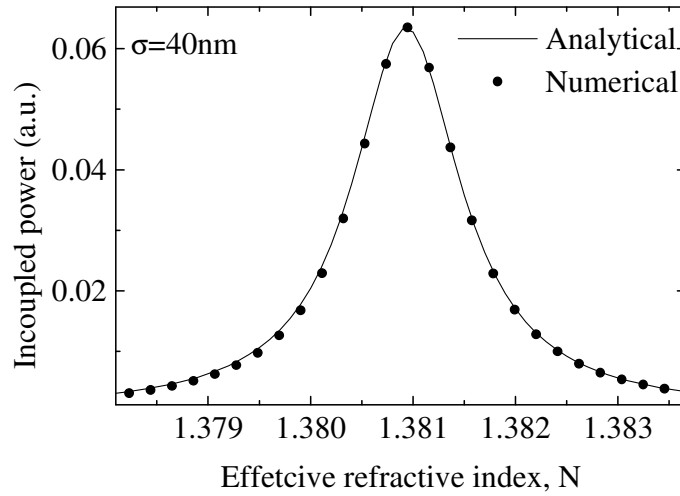


Fig. 6. Horvath et al., JOSA B

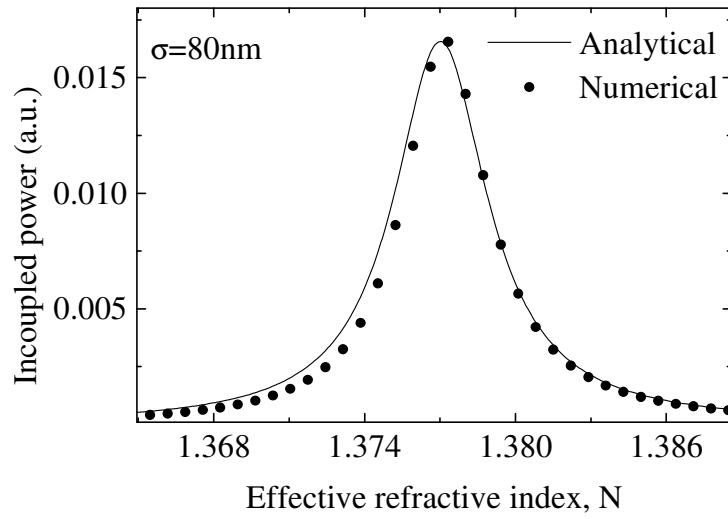


(a)



(b)

Fig. 7a,b. Horvath et al., JOSA B



(c)

Fig. 7c. Horvath et al., JOSA B

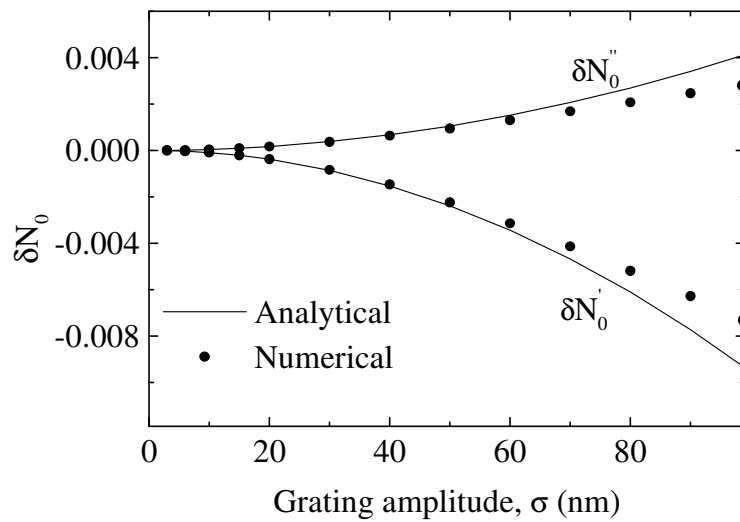


Fig. 8. Horvath et al., JOSA B